Eur. Phys. J. B **29**, 469–479 (2002)
DOI: 10.1140/epjb/e2002-00327-2

THE EUROPEAN PHYSICAL JOURNAL B

Deviations from perfect memory in spin glass temperature cycling experiments

M. Sasaki[1,a], V. Dupuis[2], J.-P. Bouchaud[2], and E. Vincent[2]

[1] Laboratoire de Physique Théorique et Modèles Statistiques, bâtiment 100, Université Paris-Sud, 91405 Orsay, France
[2] Service de Physique de l'État Condensé, Orme des Merisiers – CEA Saclay, 91191 Gif-sur-Yvette Cedex, France

Received 23 May 2002
Published online 14 October 2002 –

Abstract. We study the deviations from perfect memory in negative temperature cycle spin glass experiments. It is known that the a.c. susceptibility after the temperature is raised back to its initial value is superimposed to the reference isothermal curve for large enough temperature jumps ΔT (perfect memory). For smaller ΔT, the deviation from this perfect memory has a striking non monotonous behavior: the 'memory anomaly' is *negative* for small ΔT's, becomes positive for intermediate ΔT's, before vanishing for still larger ΔT's. We show that this interesting behavior can be reproduced by simple Random Energy trap models. We discuss an alternative interpretation in terms of droplets and temperature chaos.

PACS. 75.50.Lk Spin glasses and other random magnets – 05.70.Fh Phase transitions: general studies – 64.70.Pf Glass transitions

1 Introduction

It is well known that in glassy systems, dynamical effects strongly depend on the history of the system after quenching from above the glass transition temperature T_g. These phenomena are called aging and have been studied using various experimental protocols [1–3]. The measurement of the ac-susceptibility during negative T-cycles is one of them. This experiment consists of the following three stages. In the first stage, the system is quenched from above its critical temperature T_g and it is kept at a temperature T_1 ($< T_g$) during a time $t_{\rm w1}$. In the second stage the temperature is temporally reduced to $T_2 = T_1 - \Delta T$ during a time $t_{\rm w2}$, and then it is set back to T_1 in the third stage. The ac-susceptibility (magnetic, dielectric, mechanical, ...) is measured during all the three stages. The effect of the perturbation of the temperature is examined by comparing the perturbed and unperturbed (*i.e.* $t_{\rm w2} = 0$) data in the third stage. From this comparison, it is revealed that the perturbed data quickly approaches the unperturbed one as if the system remembers how far the relaxation at the temperature T_1 had proceeded before the perturbation, even though the system is strongly *rejuvenated* at temperature T_2 (see Fig. 1). This phenomenon is called the memory effect, and has been observed in many glassy systems like spin glasses [4–7], orientational glasses [8–10], polymer glasses [11], etc.

In the present paper, we focus on the deviations from perfect memory that are observed immediately after heating back the system to T_1. Surprisingly, systematic experiments (that we report in Sect. 2) show that the transient behavior is non monotonous as a function of ΔT. The initial extra contribution, that we will call the memory anomaly, is found to be *negative* for small ΔT, then *positive* for intermediate ΔT, before vanishing completely for large enough ΔT (perfect memory).

We then measure the ac-susceptibility for a T-cycle in the Random Energy Model (REM) [12] or the Generalized REM (GREM)[13]. These models have been shown [14–19] to reproduce many of the experimental features of aging, including rejuvenation and memory. We find that the non monotonous transients mentioned above can also be obtained in such models. Note that rejuvenation and memory effects can be expected from the existence of well-separated time scales [20,21] as obtained in the mean-field theory of spin glasses [22]. Also, from a microscopic point of view, it has been shown that these effects can be a direct consequence of frustrated and widely distributed interactions [23].

Technically, we first establish a relation between the ac-susceptibility and the distribution of relaxation times. Although this relation could not be derived analytically, numerical tests suggest that this relation holds with high accuracy. This enables us to measure the ac-susceptibility for any desired time scale in the REM (but not in the GREM), allowing us to measure the ac-susceptibility in

[a] e-mail: sasaki@ipno.in2p3.fr

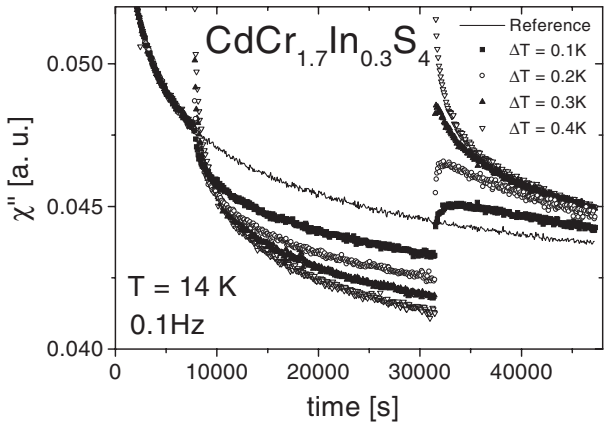

Fig. 1. Out-of-phase susceptibility χ'' *vs.* time for temperature cycling experiments at $T_1 = 14$ K on the $CdCr_{1.7}In_{0.3}S_4$ Heisenberg spin glass ($T_g = 16.7$ K). The sample was quenched to T_1, kept at this temperature during $t_1 = 7\,700$ s, and then submitted to a negative temperature cycle at $T_1 - \Delta T$ during $t_2 = 23\,650$ s before returning to T_1 for a time t_3. Four different small ΔT (0.1 K–0.4 K) were used.

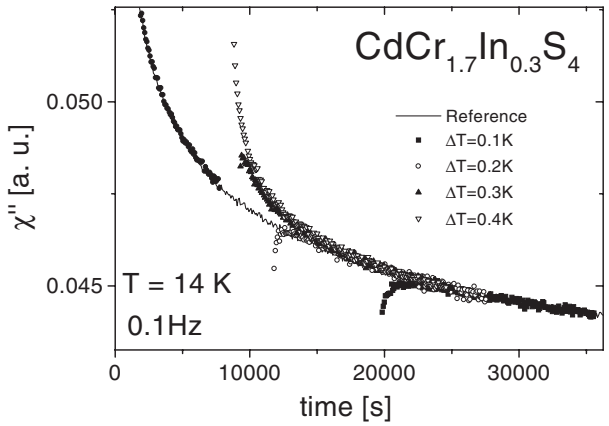

Fig. 2. Superposition of χ''-relaxations of Figure 1 after the negative temperature cycles onto a reference isothermal relaxation curve (solid line and full circles). The data measured after the cycle have been shifted horizontally by $t_2 - t_{\rm eff}$ to take into account the effective contribution $t_{\rm eff}$ of aging at $T_1 - \Delta T$ on aging at T_1. The merging of the data points with the reference curve occurs first from below for small ΔT's and then from above for larger ΔT's.

the REM up to time scales comparable to experiments. This would not be possible using Monte Carlo simulations. As for the GREM, the ac-susceptibility is obtained using Monte Carlo simulation, and therefore corresponds to rather small time scales. Our numerical measurements are made for various sets of parameters, *i.e.*, the waiting times $t_{\rm w1}$ and $t_{\rm w2}$, the temperatures T_1, T_2 and the period of the applied ac-field $P = 2\pi/\omega$. We find that the non monotonous effect described above depends quite sensitively on some of these parameters.

The organization of this manuscript is as follows: In Section 2 results of new complete set of T-cycle experiments in spin glasses are shown. In Section 3 we explain the REM, the GREM and the dynamics employed for these models. In Section 4 a relation between ac-susceptibility and distribution of relaxation times is proposed and its validity is tested numerically. In Section 5 and 6 results on the REM and on the GREM are shown. Finally, in Section 7, we give a physical discussion of our results and a comparison with the scenario of temperature chaos, where the existence of an overlap length is assumed.

2 Results of experiments

The effect of temperature changes on aging has already been largely investigated experimentally in spin glasses [1]. Here we focus on the details of the experimental results in the well characterized thiospinel $CdCr_{1.7}In_{0.3}S_4$ ($T_g = 16.7$ K) Heisenberg spin glass sample. Figure 1 presents the results on the out-of-phase component of χ'' of the a.c. susceptibility during the temperature cycle described in the introduction, with $T_1 = 14$ K, for four ΔT values in the range (0.1 K–0.4 K), and a frequency 0.1 Hz. Note that the period of the a.c. field (10 s) is typically much larger than any microscopic time scale (10^{-12} s)[1].

Just after the initial quench, χ'' is slowly relaxing downward with time $t_{\rm w1}$ due to aging. When T_1 is decreased to $T_2 = T_1 - \Delta T$, we observe a jump and a strong relaxation in χ'': this is the rejuvenation effect. Despite this strong reinitialization of aging at $T_1 - \Delta T$, it is possible, when the temperature is raised back to T_1 and for large enough ΔT (≥ 2 K) [4], to find a perfect memory of the past relaxation at T_1. For large ΔT's, the relaxations at T_1 before and after the temperature cycle are in exact continuity and there is no contribution of aging at $T_1 - \Delta T$ on aging at T_1. In contrast, in the regime of small ΔT's of Figure 1, we do not find a perfect memory of aging after the temperature cycle. The χ'' relaxations after the negative cycle can still be superposed, apart from a transient contribution to be analyzed below, onto a reference isothermal relaxation at T_1 but we now need to shift the data by an effective time $t_{\rm eff} < t_{\rm w2}$ which accounts for aging during the stay at T_2 (see Fig. 2). This effective time $t_{\rm eff}$ has been recently studied in detail both experimentally [7,24] and numerically [25,26].

Coming back to the transient contribution, we see that for the smallest $\Delta T = 0.1$ K and 0.2 K used, χ'' reaches a maximum as a function of time, and merges back with the reference curve from below, while for $\Delta T = 0.3$ K and 0.4 K the maximum disappears and this return occurs from above. This is a systematic effect which is also observed at other temperatures. We have further characterized this feature by gathering the results of several negative temperature cycling experiments done on the

[1] The relevant 'microscopic' time scale may however be strongly renormalized by critical fluctuations, as recently discussed in reference [7,20,24], and can be much larger than 10^{-12} s. for T close to T_g.

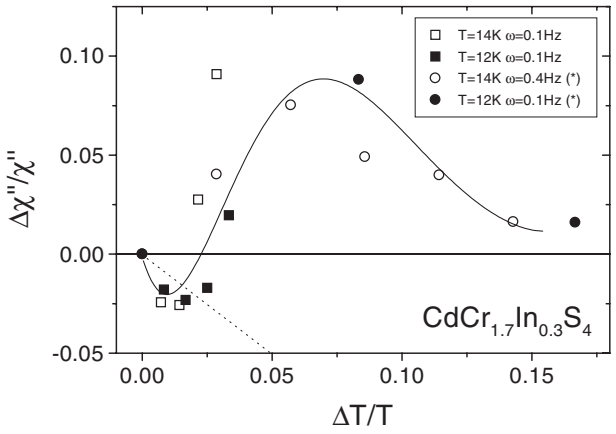

Fig. 3. Relative difference (memory 'anomaly') $\Delta\chi''/\chi''$ between the χ''-value after a negative temperature cycle of amplitude ΔT at a temperature T and the χ''-value after a corresponding isothermal aging at T during a time $t_1 + t_{\rm eff}(\Delta T)$ for various temperature cycling experiments (such as the ones presented in Figs. 1–2). The first cycles at 14 K and 12 K (0.1 Hz) correspond to $t_1 = 7\,700$ s and $t_2 = 23\,650$ s. The others (*) correspond to $t_1 = t_2 = 3\,600$ s for 14 K (0.4 Hz) and $t_1 = t_2 = 18\,000$ s for 12 K (0.1 Hz). The thin line is a guide for the eye. The dotted line corresponds to $\Delta\chi''/\chi'' = -\Delta T/T$.

Table 1. $t_{\rm eff}$: shift time (see text), t^*: position of the maximum of χ'', $t_{\rm rec.}$: time at which the signal merges with the shifted reference curve, and $\Delta\chi''/\chi''$: amplitude of the memory anomaly for different ΔT's, for $T_1 = 14$ K. The times t^* and $t_{\rm rec.}$ are counted from the last temperature shift.

ΔT (K)	$t_{\rm eff}$ (s)	t^* (s)	$t_{\rm rec.}$ (s)	$\Delta\chi''/\chi''$
0.1	12000	1800	4200	-2.4×10^{-2}
0.2	4000	900	900	-2.6×10^{-2}
0.3	1500	160	8000	2.8×10^{-2}
0.4	1000	–	10350	9.1×10^{-2}

Table 2. Same caption as Table 1 for $T_1 = 12$ K.

ΔT (K)	$t_{\rm eff}$ (s)	t^* (s)	$t_{\rm rec.}$ (s)	$\Delta\chi''/\chi''$
0.1	15000	1200	2850	-1.8×10^{-2}
0.2	8000	1200	2700	-2.3×10^{-2}
0.3	4000	800	800	-1.7×10^{-2}
0.4	2700	–	5300	2.0×10^{-2}

thiospinel sample at two temperatures $T_1 = 12$ K and $T_1 = 14$ K and for various ΔT's. In Figure 3, we have plotted the (relative) memory 'anomaly' $\Delta\chi''/\chi''$, where $\Delta\chi''$ is the difference between the χ''-value just after the cycle and the one corresponding to an isothermal aging at T during $t_{\rm w1} + t_{\rm eff}$, as a function of $\Delta T/T_1$ for the whole set of available experimental results. The characteristic time scales are given in Tables 1 and 2.

For small ΔT's, $\Delta\chi''/\chi''$ is negative and χ'' approaches the reference curve from below. As ΔT increases, this ratio becomes positive meaning that the approach takes place now from above the reference curve (Fig. 2). For larger ΔT's, $\Delta\chi''/\chi''$ shows a maximum and decreases back towards zero. Beyond that point, rejuvenation and full memory effects are observed [27] and aging at T_2 has no influence on the aging at T_1. This characteristic oscillation of $\Delta\chi''/\chi''$ as a function of ΔT is the central result of this paper, that we discuss below in the context of Random Energy Models. It is worth noticing that in the measurement of d.c. magnetization with T-cycle, the relaxation rate $S(t)$ at a short fixed time shows a similar non monotonous behavior on ΔT [28]. This is quite reasonable if we notice the rough relation $\chi''(\omega) \sim S(\omega^{-1})$ (we thank P. Nordblad for pointing this out).

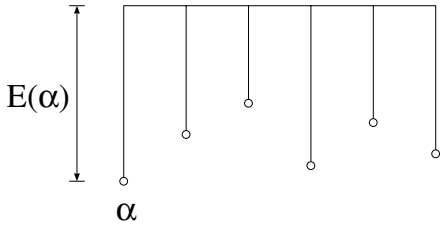

Fig. 4. Structure of the Random Energy Model.

The time t^* at which the maximum of χ'' occurs rapidly decreases as ΔT increases, whereas the recovery time $t_{\rm rec.}$ at which the signal merges with the shifted reference curve has a non monotonous behavior with ΔT (see Tabs. 1 and 2). For still larger ΔT's, this time decays back to zero. In addition, quite surprisingly, $t_{\rm rec.}$ is very long for intermediate ΔT's – much longer than expected from activated thermal slowing down. This *second non monotonous behavior* of $t_{\rm rec.}$ and the unexpected long $t_{\rm rec.}$ will be reconsidered in Section 7.

3 Models

This section is devoted to introducing the REM, the GREM and their dynamical extensions. A magnetization-like variable is introduced in order to define and measure an ac-susceptibility.

3.1 The REM

The REM is schematically shown in Figure 4. The bottom points are the accessible states of the system. We will consider the case where N, the total number of states, is very large. Each branch represents the barrier energy E, over which the system goes from one state to another. The values of E are assigned randomly and independently according to the distribution :

$$\rho(E)\mathrm{d}E = \frac{\mathrm{d}E}{T_g}\exp[-E/T_g] \qquad (E \geq 0), \qquad (1)$$

where T_g is the transition temperature of the model. Hereafter T_g is used as the unit of temperature and is set to 1.

From the Arrhenius law, the escape time $\tau(\alpha)$ is related to $E(\alpha)$ as

$$\tau(\alpha) = \tau_0 \exp[E(\alpha)/T], \qquad (2)$$

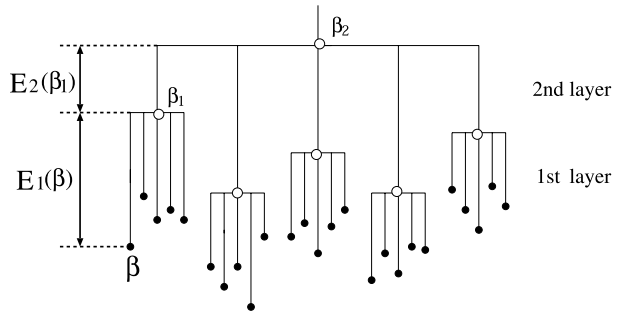

Fig. 5. Structure of the Generalized Random Energy Model with $L = 2$.

where T is the temperature and τ_0 is a microscopic time scale. Hereafter τ_0 is used as the unit of time and is set to 1. From equation (1), the distribution of τ is

$$p_x(\tau)\mathrm{d}\tau = \frac{x}{\tau^{x+1}}\mathrm{d}\tau \qquad (\tau \geq 1), \tag{3}$$

where $x \equiv T/T_g$. From equation (3), it is clear that the averaged relaxation time is $x/(x-1)$ for $x > 1$ and infinite for $x \leq 1$. This means that the transition from an ergodic phase to a non-ergodic phase occurs at T_g [14].

We define the dynamics of the REM from a simple Markoff process that defines a 'trap' model (see also [29]). At $t = 0$, an initial state β is chosen according to the uniform distribution over all states, *i.e.*,

$$P_\alpha(0) = \frac{1}{N}\cdot \tag{4}$$

This means that the system is quenched from an infinitely high temperature. After the initial state is chosen, the system successively changes its state by repeating the following two processes.

1. The system is activated from the present state β with probability $\tau(\beta)^{-1}$ per unit time.
2. After the activation from β, the system falls in one of all the states with uniform probability.

When a magnetic field $H(t)$ is applied, the energy of a state β is shifted by $-H(t)M_\beta$ and the activation energy changes from $E(\beta)$ to $E(\beta) + H(t)M_\beta$, where M_β is the magnetization of a state β. This is the only effect of the magnetic field that we consider. The values of the magnetizations M_β are assigned randomly and independently from a given distribution $D(M)$ with zero mean.

3.2 The GREM

The GREM is schematically shown in Figure 5. This model is generated by piling up L different REM's in a hierarchical way. The energy of a branch in the nth layer (n is counted from the bottom), E_n, are given according to the distribution

$$\rho_n(E_n)\mathrm{d}E_n = \frac{\mathrm{d}E_n}{T_g(n)}\exp[-E_n/T_g(n)] \qquad (E_n \geq 0). \tag{5}$$

The transition temperatures for the layers are chosen so as to satisfy

$$T_g(1) < T_g(2) < \cdots < T_g(L). \tag{6}$$

Therefore, in this model, the system freezes progressively from the uppermost (the Lth) layer to the lowest one as the temperature decreases.

Now let us turn to the dynamics of the GREM. The initial state is given in the same way as the REM, *i.e.*, equation (4). After the initial state is chosen, the system successively changes its state by repeating the following two processes.

1. The system is activated from the present state β to its kth ancestor β_k (see Fig. 5) with the probability

$$W(\beta;k) = \left[\tau_0^{-1}\prod_{i=1}^{k}\exp[-E_i(\beta_{i-1})/T]\right] \times\left[1-\exp[-E_{k+1}(\beta_k)/T]\right], \tag{7}$$

   per unit time. By convention, $E_{L+1}(\beta_L) \equiv \infty$. The first factor in the right hand represents the probability that the system is activated from β to β_k and the second one insures that the transition from β_k to β_{k+1} is not active.
2. After the activation from β to β_k, the system falls to one of all the states "under" β_k with uniform probability.

When magnetic field $H(t)$ is applied, $E_1(\beta)$ in equation (7) is replaced by $E_1(\beta) + H(t)M_\beta$. In order for nearby states to have strongly correlated magnetizations, the value of magnetization of a state β is assigned to be

$$M_\beta = \mathcal{M}_1(\beta) + \mathcal{M}_2(\beta_1) + \cdots + \mathcal{M}_L(\beta_{L-1}), \tag{8}$$

where $\mathcal{M}_{k+1}(\beta_k)$ is the contribution from the branching point β_k. The value of $\mathcal{M}_k$ is assigned independently and randomly from a given distribution $D_k(\mathcal{M}_k)$ with zero mean. If the distance $d(\alpha,\beta)$ between α and β is k, *i.e.*, $\alpha_n = \beta_n$ for $n \geq k$, the correlation between M_α and M_β comes from the common contributions of $\mathcal{M}_n$ ($n \geq k+1$) to these magnetizations, and is given by

$$\overline{M_\alpha M_\beta} = \sum_{n=k+1}^{L}\overline{\mathcal{M}_n^2}, \tag{9}$$

where $\overline{\mathcal{M}_n^2}$ is the variance of $D_n(\mathcal{M}_n)$. It decreases monotonically as k increases and thus as the barrier between the two states becomes higher, just as occurs in the SK model [30].

4 Estimates of the a.c.-susceptibility

Before we show our results, let us explain how we measure the ac-susceptibility. One simple way is to perform

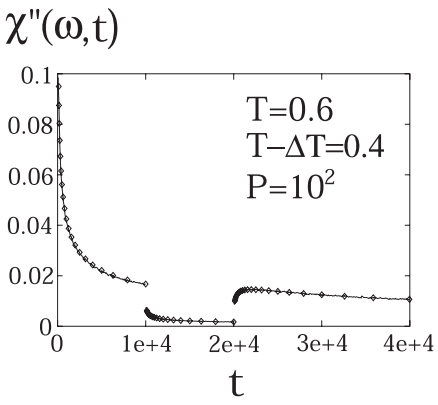

Fig. 6. The REM out-of-phase ac-susceptibility $\chi''(\omega, t)$ after a negative T-cycle. It is measured in two different ways. One can measure $\chi''(\omega, t)$ directly by a Monte Carlo simulation (the lines). The other way is to measure $\chi''(\omega, t)$ using the relation equation (10) (the diamonds). After the system is quenched from an infinitely high temperature, the temperature is changed as $T_1 = 0.6 \rightarrow T_2 = 0.4 \rightarrow T_1$. The period of the applied ac-field P is 100, and its amplitude is $0.1T_g$. For the data obtained by Monte Carlo simulation, an average is taken over 2×10^7 samples.

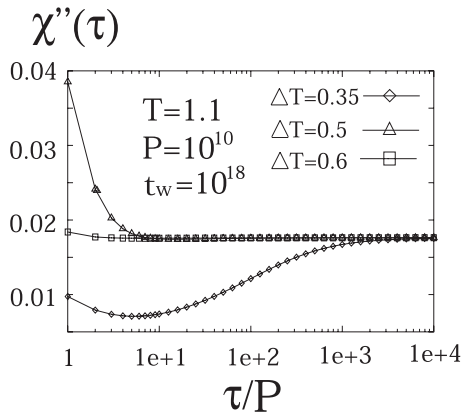

Fig. 7. The REM out-of-phase ac-susceptibility χ'' after a negative T-cycle, plotted as a function of τ/P, where τ is the time elapsed after the temperature is returned to T_1 and P is the period of the applied ac-field. After the system is quenched from an infinitely high temperature, it is kept at $T_1 = 1.1$ for $t_w = 10^{18}$. Then the temperature is reduced to $T_1 - \Delta T$ for t_w, and is then shifted back to T_1. The period of the applied ac-field is $P = 10^{10}$.

a Monte Carlo simulation. But the time scale for which we can study by Monte Carlo simulation is quite different from the experimental one. For example, if we measure the period of the applied ac-field in units of the microscopic time of the system, a typical value in numerical studies is 10^2 (see Refs. [16,19,25,31,32]), while that in experiments is $10^6 - 10^{12}$ (in the vicinity of T_g, the microscopic time scale may be renormalized by critical fluctuations: see Refs. [4,5,7]).

In the case of the REM, we can overcome this problem by using the relation

$$\chi(\omega, t) \approx \frac{\overline{M^2}}{T} \int \frac{1}{1 - \mathrm{i}\omega\tau} Q(\tau, t) \mathrm{d}\tau, \qquad (10)$$

where ω is the angular frequency of the ac-field, $\overline{M^2}$ is the variance of $D(M)$ and $Q(\tau, t)$ is the probability density that the system is found at time t in one of the states whose relaxation time is τ. In equation (10), both $\chi(\omega, t)$ and $Q(\tau, t)$ are the disorder averaged quantities. The merit of this method is that we can calculate $Q(\tau, t)$ at arbitrary time t for arbitrary initial condition $Q(\tau, t = 0)$ because the Green function $G_{\beta\alpha}(t)$, *i.e.*, the probability that the system which initially is at α reaches β at time t, has already been calculated analytically in reference [15]. As a result, we can estimate ac-susceptibility even for very long time scales comparable to those in experiments. The details of how we can calculate $Q(\tau, t)$ are described in the Appendix.

Here the question is whether the relation equation (10) is valid or not even if the system is not equilibrated. In order to examine this question, we compared data obtained by Monte Carlo simulation and those obtained by equation (10). One example is shown in Figure 6. A negative T-cycle is applied during the measurement. The agreement between both data is almost perfect. We also checked that both data coincide very well also for the in-phase ac-susceptibility χ'. We can therefore trust the validity of equation (10) for our purposes.

Concerning the GREM, $\chi(\omega, t)$ has been measured by Monte Carlo simulation because we have not succeeded in calculating $Q(\tau, t)$ analytically.

5 Results for the REM

In this section, the results of ac-susceptibility measurements during a T-cycle in the REM are shown. The measurement is done in the following way: After the system is quenched from an infinitely high temperature, the temperature is kept at T_1 in the first stage. In the subsequent second stage the temperature is reduced to $T_2 \equiv T_1 - \Delta T$, and then it is returned to T_1 in the third stage. The time t_{w1} of the first stage and that of the second stage (t_{w2}) are taken to be equal for simplicity: $t_{w1} = t_{w2} = t_w$. The ac-susceptibility $\chi(\omega, t)$ is estimated by (10) with $\overline{M^2} = 1$.

5.1 The case $T_1 > T_g$

5.1.1 Results

In Figure 7, out-of-phase ac-susceptibility χ'' for $T_1 = 1.1$ and $t_w = 10^{18}$ is plotted as a function of τ/P, where τ is elapsed time in the third stage and P is the period of the applied ac-field. The value of P is 10^{10}. We find that χ'' approaches its equilibrium value χ''_{eq} from below for small ΔT, it approaches from above for intermediate ΔT, and $\chi'' \approx \chi''_{eq}$ from the beginning of the third stage for large ΔT. This is exactly what is observed in experiments. In Figure 8, we plot

$$\Delta\chi'' \equiv \chi''(t = 2t_w + P) - \chi''(t = t_w), \qquad (11)$$

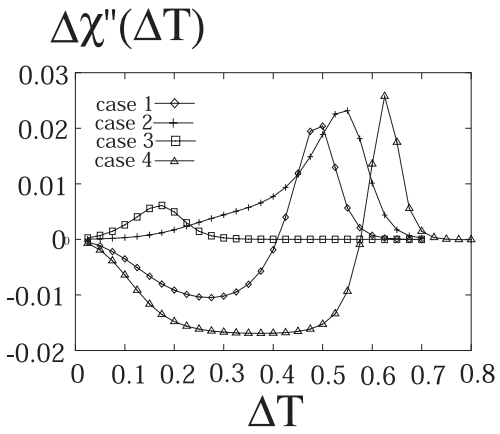

Fig. 8. $\Delta\chi''$ measured in the REM, plotted as a function of ΔT (see Eq. (11) for the definition of $\Delta\chi''$). The values of the temperature T_1, the period of the applied ac-field P and the waiting time $t_{\rm w}$ are $(T_1, P, t_{\rm w}) = (1.1, 10^{10}, 10^{18})$ for case 1, $(T_1, P, t_{\rm w}) = (1.25, 10^{10}, 10^{18})$ for case 2, $(T_1, P, t_{\rm w}) = (1.1, 10^{15}, 10^{18})$ for case 3 and $(T_1, P, t_{\rm w}) = (1.1, 10^{10}, 10^{23})$ for case 4.

as a function of ΔT by the diamonds (case 1). We can easily find the similarity between this curve and the experimental one shown in Figure 3.

Now let us change one of the three parameters T_1, P and $t_{\rm w}$ and see how these changes affect the result. First, $\Delta\chi''$ when only T_1 is changed from 1.1 to 1.25 is shown in Figure 8 by the crosses (case 2). The behavior is quite different from that observed in the case 1 above, *i.e.*, $\Delta\chi'' > 0$ for all ΔT's. Next, $\Delta\chi''$ when only P is changed from 10^{10} to 10^{15} is shown by the squares (case 3). We again find that $\Delta\chi'' > 0$ for all ΔT's. Finally, $\Delta\chi''$ when only $t_{\rm w}$ is changed from 10^{18} to 10^{23} is shown by the triangles (case 4). Although the value of ΔT above which $\Delta\chi'' \approx 0$ becomes large, there are not qualitative differences in comparison with case 1. Therefore, the non monotonous transient effect disappears (i) at low frequencies and (ii) when the initial temperature is not close enough to T_g.

5.1.2 Qualitative discussion

In order to understand these surprising results, let us investigate the time dependent energy distribution $P(E,t)$ which is related to $Q(\tau,t)$ through the relation

$$P(E,t)|{\rm d}E| = Q(\tau,t)|{\rm d}\tau|, \tag{12}$$

and equation (2). In Figure 9, $P(E,t)$ at $t = 2t_{\rm w} + P$ (*i.e.* in the third part of the cycle, after one period of the a.c. field) is plotted for six different values of ΔT (the thick line). The parameters T_1, $t_{\rm w}$ and P are the same as those of the case 1 in Figure 8. For comparison, a function which is proportional to

$$\Omega(E) \equiv \frac{\omega\tau}{1+(\omega\tau)^2} = \frac{(\frac{2\pi}{P})\exp(E/T)}{1+(\frac{2\pi}{P})^2\exp(2E/T)}, \tag{13}$$

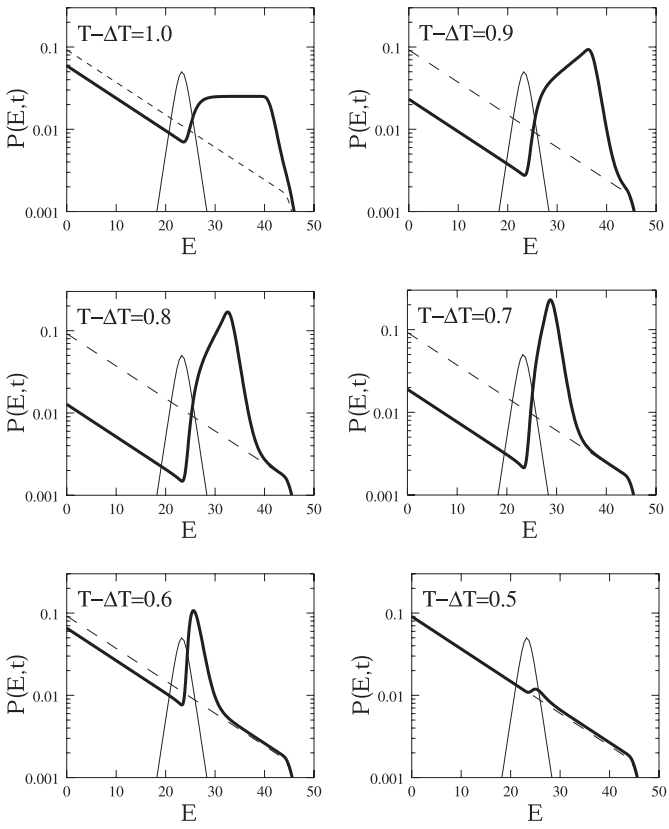

Fig. 9. The energy distribution $P(E,t)$ in the REM at time $t = 2t_{\rm w} + P$ after a negative T-cycle (the thick line). The values of parameter T, P and $t_{\rm w}$ are the same as those of the case 1 in Figure 8. For comparison, a function proportional to $\Omega(E)$ (see Eq. (13)) and $P(E,t_{\rm w})$ at $t = t_{\rm w}$ are drawn by the thin line and the broken one, respectively.

and $P(E,t)$ at $t = t_{\rm w}$ are drawn by the thin line and the broken one, respectively. It is worth noticing that the data of case 1 in Figure 8 are obtained by integrating $P(E, t = 2t_{\rm w} + P)\Omega(E)$ over E. From this figure, we find that $P(E,t)$ has both a minimum and a maximum as a function of E (or a plateau in the special case $T_1 - \Delta T = 1.0$).

When the system is kept at a temperature T for a time t, the equilibration at T proceeds and $P(E,t)$ becomes proportional to $\exp[\lambda_{\rm eq}(T)E]$ with

$$\lambda_{\rm eq}(T) = \frac{1}{T} - \frac{1}{T_g}, \tag{14}$$

for $0 \le E \le T\log(t)$. Therefore, $P(E,t)$ is equilibrated up to the energy:

$$E_2 \approx (T_2)\log(t_{\rm w}), \tag{15}$$

in the second stage. When the temperature is returned to T_1, the re-equilibration at temperature T_1 starts and it proceeds up to

$$E_3 \approx T\log(P), \tag{16}$$

at time $t = 2t_{\rm w} + P$. These considerations naturally lead us to the approximate shape of the energy distribution:

$$P(E, 2t_{\rm w} + P) \propto \begin{cases} \exp[\lambda_{\rm eq}(T_1)E] \ (0 \le E \le E_3), \\ \exp[\lambda_{\rm eq}(T_2)E] \ (E_3 \le E \le E_2), \end{cases} \tag{17}$$

provided $E_3 < E_2$. Accordingly, a minimum around $E \approx E_3$ and a maximum around $E \approx E_2$ appear for $T_2 < 1.0$, and there is a plateau between E_3 and E_2 for $T_2 = 1.0$. As for the case $T_2 = 0.5$, the peak is erased since in this case $E_2 < E_3$.

From Figure 9, the result of the case 1 in Figure 8 is understood as follows. Because of the existence of a peak (or a plateau) and the normalization of $P(E,t)$ with respect to E, the difference $P(E, t = 2t_{\rm w} + P) - P(E, t = t_{\rm w})$ changes its sign at a certain point E_*, which is slightly greater than E_3. Figure 9 shows that the peak around E_2 grows as ΔT increases. If we take the normalization condition into account, we notice that the growth of the peak means a decrease of $P(E, t = 2t_{\rm w} + P)$ for $E < E_*$, and a corresponding increase of the quantity $\Delta\chi''_-(\Delta T)$, defined as

$$\Delta\chi''_-(\Delta T) \equiv \int_0^{E_*} {\rm d}E\Omega(E)\Big|P(E, 2t_{\rm w} + P) - P(E, t_{\rm w})\Big|. \tag{18}$$

On the other hand, if ΔT is not very large and the location of the peak is not close to E_3, the second contribution $\Delta\chi''_+(\Delta T)$, defined as:

$$\Delta\chi''_+(\Delta T) \equiv \int_{E_*}^{\infty} {\rm d}E\Omega(E)\Big|P(E, 2t_{\rm w} + P) - P(E, t_{\rm w})\Big|, \tag{19}$$

cannot be very large (note that the peak of $\Omega(E)$ is around E_3). As a result, $\Delta\chi'' = \Delta\chi''_+ - \Delta\chi''_-$ is negative for small ΔT (see Fig. 10 where $\Delta\chi''_+(\Delta T)$ and $\Delta\chi''_-(\Delta T)$ for case 1 are plotted by the diamonds). Then, as ΔT increases, the location of the peak approaches E_3 and $\Delta\chi''_+(\Delta T)$ increases. Therefore, $\Delta\chi''(\Delta T)$ is positive for intermediate ΔT. This peak disappears when ΔT is large and $E_2 < E_3$. This is the reason why $\Delta\chi''(\Delta T) \approx 0$ for large ΔT.

Our next interest is to understand the following two trends:

(i) If either the temperature or the period of the applied ac-field is large enough, $\Delta\chi''(\Delta T) > 0$ for all ΔT.
(ii) The behavior of $\Delta\chi''(\Delta T)$ does not depend sensitively on $t_{\rm w}$, except that the value of ΔT above which $\Delta\chi'' \approx 0$ increases with $t_{\rm w}$.

To understand these trends, an important point is to note that $\Delta\chi''_-(\Delta T)$ satisfies the inequality

$$\begin{aligned} \Delta\chi''_-(\Delta T) &< \int_0^{\infty} {\rm d}E\Omega(E)P(E, t = t_{\rm w}) \\ &\approx \int_0^{\infty} {\rm d}E\lambda_{\rm eq}(T)\exp[\lambda_{\rm eq}(T)E]\Omega(E) \\ &\sim P^{\frac{T_g - T}{T_g}}. \end{aligned} \tag{20}$$

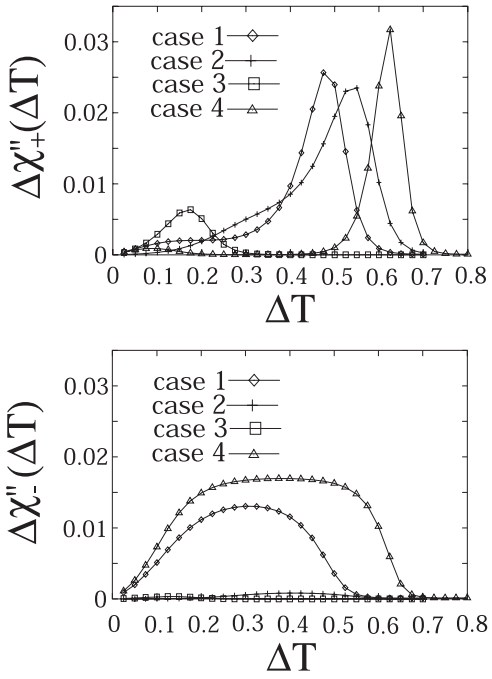

Fig. 10. The functions $\Delta\chi''_+(\Delta T)$ and $\Delta\chi''_-(\Delta T)$ in the REM for each of the cases of Figure 8 are plotted as a function of ΔT. See equations (18) and (19) for the definitions of $\Delta\chi''_+$ and $\Delta\chi''_+$.

It is obvious from this inequality that $\Delta\chi''_-(\Delta T)$ is a decreasing function of T and P. The quantity $\Delta\chi''_+(\Delta T)$, on the other hand, does not depend strongly on either T or P. This explains point (i) above.

On the other hand, there is no $t_{\rm w}$ dependence in the inequality (20). This is the reason why behavior of $\Delta\chi''(\Delta T)$ does not depend on $t_{\rm w}$ so much. However, the value of ΔT above which $\Delta\chi'' \approx 0$ increases with increasing $t_{\rm w}$ because it is determined from the condition:

$$E_2 \approx E_3. \tag{21}$$

The explanation for these two trends is confirmed by Figure 10, where $\Delta\chi''_+(\Delta T)$ and $\Delta\chi''_-(\Delta T)$ in each of the cases of Figure 8 are plotted as a function of ΔT. The function $\Delta\chi''_+(\Delta T)$ does not depend much on the parameters T, P and $t_{\rm w}$ compared to $\Delta\chi''_-(\Delta T)$, which becomes rather small when either T or P is large enough.

5.2 The case $T_1 < T_g$

Figure 11 shows $\Delta\chi''_+$ and $\Delta\chi''_-$ in the case $T_1 = 0.8$, $P = 10^{10}$ and $t_{\rm w} = 10^{18}$. Because χ'' decreases towards zero with time for $T < T_g$, we change slightly the definition of $\Delta\chi''_+$ and that of $\Delta\chi''_-$ and replace $P(E, t = t_{\rm w})$ in equations (18) and (19) with $P_{\rm const}(E, t = t_{\rm eff})$, where $P_{\rm const}(E,t)$ is isothermal energy distribution at T_1, and $t_{\rm eff}$ is estimated as

$$t_{\rm eff} = t - t_{\rm w} + (t_{\rm w})^{T_2/T_1}. \tag{22}$$

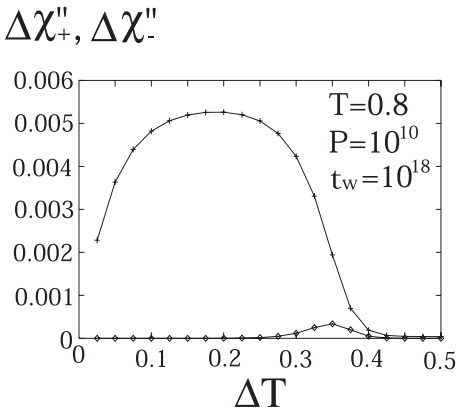

Fig. 11. The functions $\Delta\chi''_+$ (the diamonds) and $\Delta\chi''_-$ (the crosses) in the REM for the case $T_1 = 0.8$, $P = 10^{10}$ and $t_w = 10^{18}$. The definition of $\Delta\chi''_+$ and that of $\Delta\chi''_-$ are slightly changed by replacing $P(E, t = t_w)$ in equations (18) and (19) with $P_{\rm const}(E, t = t_{\rm eff})$, where $P_{\rm const}(E, t)$ is isothermal energy distribution at T and $t_{\rm eff}$ is defined by equation (22).

It is worth noticing that the effective time in the second stage is estimated as $(t_w)^{T_2/T_1}$. It has been shown in reference [17] that this way to estimate the effective time works well in the REM. The result is similar to that of the case $T_1 > T_g$ shown in Figure 8 in the sense that $\Delta\chi''_-$ has a wide plateau and $\Delta\chi''_+$ has a peak around the value of ΔT at which equation (21) is satisfied (in this case the value is about 0.356). The only difference is that $\Delta\chi''_+$ now never exceeds $\Delta\chi''_-$, so that $\Delta\chi''$ is negative for all ΔT.

The dependence on the different parameters was also investigated by changing one of the three parameters T, P and t_w. The ranges we examined are $0.75 \leq T_1 \leq 0.9$, $10^{10} \leq P \leq 10^{15}$ and $10^{18} \leq t_w \leq 10^{23}$, respectively. As a result, we found that $\Delta\chi''_- > \Delta\chi''_+$ is always satisfied for all ΔT in all the cases. Therefore, the condition $T_1 > T_g > T_2$ is required to observe a non monotonous memory anomaly.

6 Results for the GREM

Now let us turn our attention to the GREM. As mentioned in Section 4, $\chi(\omega, t)$ for the GREM has been measured using Monte Carlo simulation because we have not succeeded in calculating $Q(\tau, t)$ analytically. However, we do not measure $\chi(\omega, t)$ from the linear response to an ac-field because this procedure requires averaging over a very large number of samples (typically $10^7 - 10^8$ samples). Instead, we have estimated the ac-susceptibility from the relations:

$$\chi_k(\omega, t) = \frac{\overline{\mathcal{M}_k^2}}{T} \int \frac{1}{1 - \mathrm{i}\omega\tau_k} Q_k(\tau_k, t) \mathrm{d}\tau_k, \qquad (23)$$

where

$$\tau_k \equiv \exp\left[\frac{\sum_{i=1}^{k} E_i}{T}\right], \qquad (24)$$

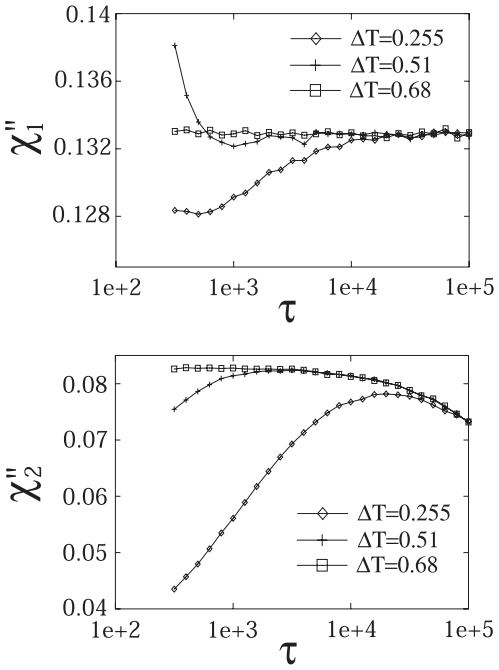

Fig. 12. The GREM out-of-phase ac-susceptibility χ''_k after a negative T-cycle as a function of the elapsed time τ after the temperature is returned to T_1. This GREM has $L = 2$, $T_g(1) = 0.5$ and $T_g(2) = 1.0$. The period of the applied ac-field is $P = 3 \times 10^2$, and its amplitude is $0.1T_g(2)$. After the system is quenched from an infinitely high temperature, the temperature is kept at $T_1 = 0.85$ for $t_w = 10^5$ in the first stage. In the second stage the temperature is temporally reduced to $T_1 - \Delta T$ for the same time t_w, and before being returned to T_1 in the last stage.

the function $Q_k(\tau, t)$ is the probability density of τ_k at time t and $\chi_k(\omega, t)$ is ac-susceptibility calculated from $\mathcal{M}_k$. It is this probability density $Q_k(\tau_k, t)$ that we obtained from Monte Carlo simulation. The validity of these relations was confirmed numerically by comparing data from the direct measurement of $\mathcal{M}_k$ under an ac-field and from equation (23).

Because we have to rely on Monte Carlo simulation, the time scales are rather restricted as compared to the REM. Therefore, we will confine ourselves to showing results with one set of parameters. The system we have investigated is the GREM with $L = 2$ (L is the number of layers), $T_g(1) = 0.5$ and $T_g(2) = 1.0$. The disorder average is taken over 8×10^6 samples. The period of the applied ac-field is 300. After the system is quenched from an infinitely high temperature, the temperature is kept at $T_1 = 0.85$ for $t_w = 10^5$ in the first stage. In the subsequent second stage the temperature is reduced to T_2 for t_w, and then it is returned to T_1 in the third stage. In Figure 12, the contribution from both levels, χ''_1 and χ''_2 are plotted as a function of τ, where τ is elapsed time in the third stage. As for χ''_1, we again find a non monotonous behavior, similar to that observed in experiments (Fig. 3) and in the REM (Fig. 7). This was expected, since for the first level dynamics is very similar to the single REM, with transitions to the higher level frozen by the fact that $T_1 < T_g(2)$.

On the other hand, the memory anomaly in χ_2'' is always negative, for all values of ΔT. This result is consistent with that obtained in the REM where χ'' always approaches the reference curve from below if $T_1 < T_g$ (note that $T_1 < T_g(2)$ in the present case).

Finally, let us discuss what would happen in the case $L \gg 1$. There, some layers are frozen ($T < T_g(n)$) and others layers are *fast* ($T > T_g(n')$) at any given temperature $T < T_g = T_g(L)$. From the study on the REM shown in Section 5, we expect that the contributions to χ'' from the frozen layers will always lead to a negative memory anomaly, where as the contribution from the 'critical' levels will lead to a non monotonous contribution.

7 Discussion. Other scenarios

We have seen that the non monotonous transient effect observed in memory experiments can be reproduced within simple REM trap model, provided the temperature is above and close enough to the critical temperature and the frequency not too low. The same mechanism is present in the GREM, and is governed by the dynamics around the 'critical level', *i.e.* the level such that its critical temperature is close to the working temperature. As emphasized in references [33,20], the physical interpretation of the different 'levels' is in terms of length scales: small scale dynamics corresponds to the deepest level of the tree, whereas large length scales correspond to the upper level of the trees. The observed aging dynamics always concerns those length scales (levels) around the critical temperature: larger length scales are frozen, whereas smaller length scales are completely equilibrated. Hence, in the above GREM interpretation, the important ingredient is that the system remains close to criticality at any temperature, but the basic ingredient is already present in the REM, and is related to the abrupt change of the way the different states are explored at T_g (see [34]).

The GREM model is a concrete implementation of the so called 'hierarchical' interpretation of experimental data [35], to which one often opposes the 'droplet' interpretation [36]. As discussed in details in reference [20], the two interpretations are to some extent complementary if one wants to interpret the 'hierarchy' of phase space as a hierarchy of length and time scales.

However, the droplet interpretation of the rejuvenation and memory experiments makes an extra assumption that we now discuss. The existence of an overlap length $\ell_{\Delta T}$ between typical configurations at T and $T - \Delta T$ is postulated [36,37], such that for length scales larger than $\ell_{\Delta T}$, the configurations at the two temperatures are completely unrelated ('temperature chaos'). Using plausible arguments, one deduces that $\ell_{\Delta T}$ should diverge as a power-law of ΔT for $\Delta T \to 0$. Recent experimental data has given some credit to the existence of temperature chaos [38] (but see the recent discussions in [26,39,40]). After a waiting time $t_{\rm w1}$, the active length scales are such that $\tau_r(\ell_{\rm w1}, T_1) \sim t_{\rm w1}$, where $\tau_r(\ell, T)$ is the typical relaxation time corresponding to length ℓ at temperature T. Length scales much smaller than $\ell_{\rm w1}$ are fully equilibrated. In this picture, the scenario for rejuvenation is thus the following: whenever $\ell_{\rm w1} < \ell_{\Delta T}$, the temperature change does not modify the achieved pattern, but only acts to slow down the dynamics. Conversely, when ΔT is such that $\ell_{\rm w1} > \ell_{\Delta T}$, the system has to start rebuilding new correlations as if it were brought directly from high temperature (when $\ell_{\Delta T} \to 0$). As shown in details in reference [21], this does not necessarily mean that the structure grown at the first temperature is immediately washed away. On the contrary, as long as the length scales $\ell_{\rm w2}$, active at T_2, remain small compared to $\ell_{\rm w1}$, memory can be partially or totally recovered. The criterion is the following: the time needed to erase the effect of the dynamics at T_2 when the system is heated back, and isothermal dynamics at T_1 is recovered, is given by:

$$t_{\rm rec.}(t_{\rm w2}) \sim \tau_r(\ell_{\rm w2}, T_1). \tag{25}$$

Since $\ell_{\rm w2}$ decreases extremely fast with decreasing temperature [20,7,26,24,41], $t_{\rm rec.}(t_{\rm w2})$ decreases very rapidly (for a given $t_{\rm w2}$) as ΔT increases, and should soon become smaller than ω^{-1}, which is the smallest time for which a measurement of the a.c. susceptibility can be performed.

When $t_{\rm rec.}(t_{\rm w2}) > \omega^{-1}$ and $\ell_{w2} > \ell_{\Delta T}$, on the other hand, one expects to see an initial spike in the a.c. susceptibility that corresponds to the reconstruction of small length scale correlations at T_1. Schematically, the temperature chaos scenario therefore predicts that the memory anomaly $\Delta\chi$ should be zero for $\Delta T < \Delta T^*$, with $\ell_{\rm w1} = \ell_{\Delta T^*}$, positive for larger ΔT, but becoming zero again when $t_{\rm rec.}(t_{\rm w2})$ becomes shorter than ω^{-1}.

One can finally argue that the number of thermally active (equilibrium) droplets decreases slightly when the temperature is reduced from T_1 to T_2, thereby reducing the equilibrium a.c. susceptibility. The need to renucleate these droplets back at T_1, which also takes a time $\sim t_{\rm rec.}$, would then explain the negative contribution to the memory anomaly for small ΔT[2]. This would predict that $\Delta\chi''/\chi''_{\rm eq} \simeq -[1/T + |\Upsilon'/\Upsilon|]\Delta T$ for small ΔT, where Υ is the temperature dependent stiffness of the droplets. The experimental effect, found to be stronger than $-\Delta T/T$, is in qualitative agreement with this prediction (see Fig. 3). We have furthermore checked that the amplitude of the bump in χ'' at $t = t_{\rm w1} + t_{\rm w2}$ is of the same order as the difference between the equilibrium values of $\chi''_{\rm eq}$ at T_1 and $T_1 - \Delta T$.

However, the time $t_{\rm rec.}$ beyond which the stay at T_2 is erased does not conform to the naive estimate equation (25), since it is found to be non monotonous and much larger than expected. It is rather the position t^* of the maximum of χ'' that seems to obey to equation (25). Note that the REM scenario also predicts a monotonously decreasing recovery time $t_{\rm rec.}$ with increasing ΔT. We have at present no physical interpretation for this discrepancy.

The experimental data appears to be consistent both with the above droplet/chaos interpretation and with the hierarchical model developed in the present paper (see also

[2] Note that the negative initial contribution to $\Delta\chi$ is like the Kovacs effect in polymeric glasses [42,25,26].

the discussion in [20,38]). The present study shows explicitly that the non monotonous memory anomaly does not require the existence of an overlap length. Indeed, we argued that the REM trap model, where this overlap length is absent, is also able to reproduce qualitatively the memory anomaly if one works around the freezing temperature around which 'temperature chaos' effects are observed [34]. In the REM scenario, the positive contribution to the memory anomaly comes from an over concentration of the probability weight in deep traps at T_2 as compared to the equilibrium situation at T_1 (see the discussion in Ref. [34]). Physically, this positive contribution corresponds to a freezing at T_2 of small length scales that have to unfreeze when back at T_1, a scenario that was directly confirmed by the numerical simulations of [26] where temperature chaos is absent but rejuvenation and memory effects are clearly observed.

We wish to thank L. Berthier, J. Hammann, O. Martin and H. Yoshino for many interesting conversations. We thank P. Nordblad and H. Yoshino for very useful comments on the manuscript. M.S. acknowledges a fellowship from the French Ministry of research. M.S also would like to thank CEA Saclay for hospitality where main part of this work was performed. The LPTMS laboratory is an *Unité de Recherche de l'Université Paris XI associée au CNRS*.

Appendix

This appendix is devoted to explain in detail how we can calculate $Q(\tau,t)$. We assume that the probability $P_\alpha(t=0)$ that the system is found at a state α at time $t=0$ is given. For simplicity, let us first consider the case that the system is kept at a constant temperature T. It is easily found that $Q(\tau,t)$ is given as

$$Q(\tau,t)\mathrm{d}\tau = \sum_{\beta,\alpha} \mathrm{d}\tau \delta(\tau(\beta)-\tau) G_{\beta\alpha}(t) P_\alpha(t=0), \quad (26)$$

where $G_{\beta\alpha}(t)$ is the Green function, *i.e.*, the probability that the system which initially is at α reaches β at time t.

Now let us calculate the Green function. When the system which initially is at α reaches β at time t, there are the following two possibilities:

(i) $\alpha=\beta$ and the system has not been activated during time t.
(ii) The system is activated at t' ($<t$) and reaches β after that time.

In the case (ii), because the new state after the activation is chosen randomly from all the states, the probability that the system reaches β after the activation is $P^{\mathrm{uni}}_\beta(t-t')$, where

$$P^{\mathrm{uni}}_\beta(t) = \frac{1}{N}\sum_\gamma G_{\beta\gamma}(t), \quad (27)$$

and N is the number of states. Taking this fact into consideration and recalling that the system is activated from α with the probability $\tau(\alpha)^{-1}$, we obtain

$$G_{\beta\alpha}(t) = \delta_{\alpha\beta}\exp\left[-\frac{t}{\tau(\alpha)}\right] + \int_0^t \frac{\mathrm{d}t'}{\tau(\alpha)}\exp\left[-\frac{t'}{\tau(\alpha)}\right] P^{\mathrm{uni}}_\beta(t-t'). \quad (28)$$

The Laplace transformation of this equation leads us to

$$\hat{G}_{\beta\alpha}(s) \equiv \int_0^\infty \mathrm{d}t \exp[-st] G_{\beta\alpha}(t) = \frac{\tau(\alpha)\delta_{\alpha\beta}}{s\tau(\alpha)+1} + \frac{\hat{P}^{\mathrm{uni}}_\beta(s)}{s\tau(\alpha)+1}, \quad (29)$$

where $\hat{P}^{\mathrm{uni}}_\beta(s)$ is the Laplace transformation of $P^{\mathrm{uni}}_\beta(t)$. From this equation and the Laplace transformation of equation (27), we find

$$\hat{P}^{\mathrm{uni}}_\beta(s) = \frac{\dfrac{\tau(\beta)}{s\tau(\beta)+1}}{\displaystyle\sum_\alpha \frac{s\tau(\alpha)}{s\tau(\alpha)+1}}. \quad (30)$$

The calculation of $\hat{P}^{\mathrm{uni}}_\beta(s)$ for small s and its inverse Laplace transformation have already been done in reference [15]. The results are

$$\hat{P}^{\mathrm{uni}}_\beta(s) = \begin{cases} \dfrac{\tau(\beta)}{Nxs^x c(x)(s\tau(\beta)+1)} & (x<1), \\ \dfrac{-\tau(\beta)}{Ns\log(s)(s\tau(\beta)+1)} & (x=1), \\ \dfrac{(x-1)(s+1)\tau(\beta)}{Nxs(s\tau(\beta)+1)} & (x>1), \end{cases} \quad (31)$$

and

$$P^{\mathrm{uni}}_\beta(t) = \begin{cases} \dfrac{\int_0^t \mathrm{d}u u^{x-1}\exp[-(t-u)/\tau(\beta)]}{Nxc(x)\Gamma(x)} & (x<1), \\ \dfrac{\tau(\beta)[1-\exp[-t/\tau(\beta)]]}{\log(t)} & (x=1), \\ \dfrac{(x-1)\tau(\beta)\{1-\exp[-t/\tau(\beta)]\}}{Nx} & (x>1), \end{cases} \quad (32)$$

where $x \equiv T/T_g$ and

$$c(x) = \Gamma(x)\Gamma(1-x) = \frac{\pi}{\sin(\pi x)}. \quad (33)$$

Now let us return to the calculation of $Q(\tau,t)$. The substitution of equation (28) into equation (26) leads us to

$$Q(\tau,t) = \exp[-t/\tau]Q(\tau,0) + \int_1^\infty \mathrm{d}\tau' \int_0^t \frac{\mathrm{d}t'}{\tau'} Q^{\mathrm{uni}}(\tau,t-t')\mathrm{e}^{-\frac{t'}{\tau'}} Q(\tau',0), \quad (34)$$

where

$$Q(\tau,0)\mathrm{d}\tau \equiv \sum_{\alpha} \mathrm{d}\tau\delta(\tau(\alpha)-\tau)P_{\alpha}(t=0), \qquad (35)$$

and

$$\begin{aligned} Q^{\mathrm{uni}}(\tau,t)\mathrm{d}\tau &\equiv \sum_{\alpha} \mathrm{d}\tau\delta(\tau(\alpha)-\tau)P_{\alpha}^{\mathrm{uni}}(t) \\ &= \mathrm{d}\tau N p_x(\tau)P^{\mathrm{uni}}(\tau,t). \end{aligned} \qquad (36)$$

The function $p_x(\tau)$ is defined by equation (3). From equations (32, 34) and (36), we finally obtain

$$\begin{aligned} &Q(\tau,t)-\exp[-t/\tau]Q(\tau,0) \\ &= \begin{cases} \dfrac{p_x(\tau)\tau}{xc(x)\Gamma(x)}\displaystyle\int_1^{\infty}\mathrm{d}\tau'\int_0^t \mathrm{d}u u^{x-1}\frac{Q(\tau',0)}{\tau'-\tau} \\ \quad\times\left[\exp\left(\dfrac{u-t}{\tau'}\right)-\exp\left(\dfrac{u-t}{\tau}\right)\right] & (x<1), \\ \dfrac{p_x(\tau)\tau}{\log(t)}\displaystyle\int_0^{\infty}\mathrm{d}\tau' Q(\tau',0) \\ \quad\times\left[\left\{1-\mathrm{e}^{-\frac{t}{\tau'}}\right\}-\dfrac{\tau}{\tau'-\tau}\left\{\mathrm{e}^{-\frac{t}{\tau'}}-\mathrm{e}^{-\frac{t}{\tau}}\right\}\right] & (x=1), \\ \dfrac{(x-1)p_x(\tau)\tau}{x}\displaystyle\int_0^{\infty}\mathrm{d}\tau' Q(\tau',0) \\ \quad\times\left[\left\{1-\mathrm{e}^{-\frac{t}{\tau'}}\right\}-\dfrac{\tau}{\tau'-\tau}\left\{\mathrm{e}^{-\frac{t}{\tau'}}-\mathrm{e}^{-\frac{t}{\tau}}\right\}\right] & (x>1). \end{cases} \end{aligned} \qquad (37)$$

Next, let us consider how we can calculate $Q(\tau,t)$ when the temperature is changed discontinuously as

$$T(t)=T_i \qquad (t_i \le t \le t_{i+1}). \qquad (38)$$

The answer is rather simple. At first, we calculate $Q(\tau,t_{\mathrm{w1}})$ with some initial distribution $Q(\tau,0)$. Then, we set the new initial distribution to $Q(\tau,t_{\mathrm{w1}})$ and use equation (37) to calculate $Q(\tau,t_{\mathrm{w2}})$. We can calculate $Q(\tau,t)$ at any t by repeating this procedure.

References

1. E. Vincent, J. Hammann, M. Ocio, J.P. Bouchaud, L. F. Cugliandolo in *Proceeding of the Sitges Conference on Glassy Systems*, edited by E. Rubi (Springer, Berlin, 1996)
2. P. Nordblad, P. Svendlidh in *Spin-glasses and random fields*, edited by A.P. Young (World Scientific, Singapore, 1997)
3. M.B. Weissman, in the same book as in reference [2]
4. F. Lefloch, J. Hammann, M. Ocio, E. Vincent, Europhys. Lett. **18**, 647 (1992)
5. E. Vincent, J.P. Bouchaud, J. Hammann, F. Lefloch, Phil. Mag. B **71**, 489 (1995)
6. J.O. Andersson, J. Mattsson, P. Nordblad, Phys. Rev. B **48**, 13977 (1993)
7. V. Dupuis, E. Vincent, J.-P. Bouchaud, J. Hammann, A. Ito, H.A. Katori, Phys. Rev. B **64**, 174204 (2001)
8. F. Alberici, P. Doussineau, A. Levelut, J. Phys. I France **7**, 329 (1997)
9. F. Alberici-Kious, J.P. Bouchaud, L.F. Cugliandolo, P. Doussineau, A. Levelut, Phys. Rev. Lett. **81**, 4987 (1998)
10. P. Doussineau, T. Lacerda-Aroso, A. Levelut, Europhys. Lett **46**, 401 (1999)
11. L. Bellon, S. Ciliberto, C. Laroche, preprint `cond-mat/9905160`
12. B. Derrida, Phys. Rev. B **24** 2613 (1981)
13. B. Derrida, E. Gardner, J. Phys. C **19**, 2253 (1986)
14. J.P. Bouchaud, J. Phys. I France, **2**, 1705 (1992)
15. J.P. Bouchaud, D.S. Dean J. Phys. I France **5**, 265 (1995)
16. M. Sasaki, K. Nemoto, J. Phys. Soc. Jpn **69**, 2283 (2000)
17. M. Sasaki, K. Nemoto, J. Phys. Soc. Jpn **69**, 2642 (2000)
18. M. Sasaki, K. Nemoto, J. Phys. Soc. Jpn **69**, 3045 (2000)
19. M. Sasaki, K. Nemoto, J. Phys. Soc. Jpn **70**, 1099 (2001)
20. J.-P. Bouchaud, V. Dupuis, J. Hammann, E. Vincent, Phys. Rev. B **65**, 024439 (2002)
21. H. Yoshino, A. Lemaître, J.-P. Bouchaud, Eur. Phys. J. B **20**, 367 (2001)
22. L.F. Cugliandolo, J. Kurchan, Phys. Rev. B **60**, 922 (1999)
23. S. Miyashita, E. Vincent, Eur. Phys. J. B **22**, 203 (2001)
24. P.E. Jönsson, H. Yoshino, P. Nordblad, H. Aruga Katori, A. Ito, Phys. Rev. Lett. **88**, 257204 (2002)
25. T. Komori, H. Yoshino, H. Takayama, J. Phys. Soc. Jpn **68**, 3387 (1999); **69**, 1192 (2000); **69**, Suppl. A 228 (2000)
26. L. Berthier, J.P. Bouchaud, Phys. Rev. B **66**, 054404 (2002), and comment in preparation
27. K. Jonason, E. Vincent, J. Hammann, J.-P. Bouchaud, P. Nordblad, Phys. Rev. Lett. **81**, 3243 (1998)
28. P. Granberg, L. Lundgren, P. Nordblad, J. Magn. Magn. Mat. **92**, 228 (1990)
29. For a recent work from a more mathematical point of view, see: G. Ben Arous, A. Bovier, V. Gayrard, Phys. Rev. Lett. **88**, 087201 (2002)
30. K. Nemoto, J. Phys. A **21**, L287 (1988)
31. M. Picco, F. Ricci-Tersenghi, F. Ritort, Phys. Rev. B **63**, 174412 (2001)
32. M. Picco, F. Ricci-Tersenghi, F. Ritort, Eur. Phys. J. B **21**, 211 (2001)
33. J.-P. Bouchaud, in *Soft and fragile matter*, edited by M.E. Cates, M.R. Evans (Institute of Physics Publishing, Bristol, 2000)
34. M. Sales, J.P. Bouchaud, Europhys. Lett. **56**, 181 (2001)
35. Ph. Refregier, E. Vincent, J. Hammann, M. Ocio, J. Phys. France **48**, 1533 (1987)
36. D.S. Fisher, D.A. Huse, Phys. Rev. B **38**, 373 (1988)
37. A.J. Bray, M.A. Moore, Phys. Rev. Lett. **58**, 57 (1987)
38. P.E. Jönsson, H. Yoshino, P. Nordblad, Phys. Rev. Lett. **89**, 097201 (2002)
39. M. Sasaki, O.C. Martin, e-print `cond-mat/0206316`, to appear in Europhys. Lett.
40. T. Aspelmeier, A.J. Bray, M.A. Moore, e-print `cond-mat/0207300`
41. H. Yoshino, K. Hukushima, H. Takayama, Phys. Rev. B **66**, 064431 (2002)
42. A.J. Kovacs, Adv. Polym. Sci. **3**, 394 (1963); A.J. Kovacs *et al.*, J. Polymer Sci. **17**, 1097 (1979)